An entropy scaling demarcation of gas- and liquid-like fluid behaviors

Ian Bell, Guillaume Galliero, Stephanie Delage Santacreu, Lorenzo Costigliola

An Entropy Scaling Demarcation of Gas- and Liquid-like Fluid Behaviors

Ian H. Bell (ian.bell@nist.gov, corresponding author)*
Applied Chemicals and Materials Division, National Institute of Standards and Technology, Boulder, CO 80305

Guillaume Galliero†
Universite de Pau et des Pays de l'Adour, e2s UPPA, TOTAL, CNRS, LFCR, UMR 5150, Laboratoire des fluides complexes et leurs reservoirs, Pau, France

Stéphanie Delage-Santacreu‡
Universite de Pau et des Pays de l'Adour, e2s UPPA, Laboratoire de Mathematiques et de leurs Applications de Pau (IPRA, CNRS UMR5142), Pau, France

Lorenzo Costigliola§
Department of Science and Environment, Roskilde University, Postbox 260, DK-4000 Roskilde, Denmark

(Dated: April 10, 2020)

In this work we propose a generic and simple definition of a line separating gas-like and liquid-like fluid behaviors from the standpoint of shear viscosity. This definition is valid even for fluids like the hard sphere and the inverse power law which exhibit a unique fluid phase. We argue that this line is defined by the location of the minimum of the macroscopically scaled viscosity when plotted as a function of the excess entropy, which differs from the popular Widom lines. For hard sphere, Lennard-Jones, and inverse-power-law fluids, such a line is located at an excess entropy approximately equal to $-2/3$ times Boltzmann's constant and corresponds to points in the thermodynamic space for which the kinetic contribution to viscosity is approximately half of the total viscosity. For flexible Lennard-Jones chains, the excess entropy at the minimum is a linear function of the chain length. This definition opens a straightforward route to classify the dynamic behavior of fluids from a single thermodynamic quantity obtainable from high-accuracy thermodynamic models.

BACKGROUND

There is a long history of interest in supercritical fluid behavior, going back to Andrews' experiments with CO_2 in 1869 [1, 2]. The question of defining a metric that can be used to differentiate gas-like behavior from liquid-like behavior has seen significant interest in the intervening years. Common means of identifying the change between gas-like and liquid-like behaviors are the Widom line [3–5], extrema in thermal diffusivity and kinematic viscosity [6–8], and the Frenkel line [9–12], though each of these definitions has deficiencies.

In this work a rather different approach for demarcating gas- and liquid-like behaviors is presented and applied to hard-sphere, inverse-power-law, Lennard-Jones and flexible Lennard-Jones chain model fluids. We begin by considering the macroscopically scaled viscosity [13] for a number of atomic fluids and note that their scaled viscosity minima occur in a remarkably narrow range of excess entropy. From that insight we proceed to investigate the cause of this similarity, identifying connections between excess entropy and the kinetic and configurational contributions to the viscosity. The analysis for atomic fluids has a direct extension to molecules. Put simply, the excess entropy can be used to demarcate gas-like and liquid-like behaviors.

ENTROPY SCALING

Rosenfeld [13] laid the foundation for the field of entropy scaling of transport properties with his work four decades ago. This work has received revived interest in recent years as evidenced by a recent review on the topic [14]. The salient part of Rosenfeld's thesis is that the transport properties, when scaled by the appropriate macroscopic dimensions [15], should be a function only of the excess entropy. This conclusion was formed based on the analysis of a rather small set of molecular dynamics simulations available at the time.

The first version of isomorph theory [16–20], which is closely related to entropy scaling [14], states that *if* there are isomorphs (curves along which the macroscopically scaled structure and dynamics are constant), *then* certain properties are constant along these curves, among which are: macroscopically scaled viscosity, excess entropy, and so on [18]; not all scaled transport properties are isomorph invariants [21]. Furthermore, according to the isomorph theory, the causality does not go the other way; a line of constant excess entropy is not necessarily a line along which the macroscopically scaled viscosity is constant.

Here we define the excess entropy by

$$s^{\mathrm{ex}}(T,\rho_{\mathrm{N}}) \equiv s(T,\rho_{\mathrm{N}}) - s^{(0)}(T,\rho_{\mathrm{N}}). \tag{1}$$

where s^{ex} is the excess entropy per particle, s is the entropy per particle, $s^{(0)}$ is the ideal gas entropy per parti-

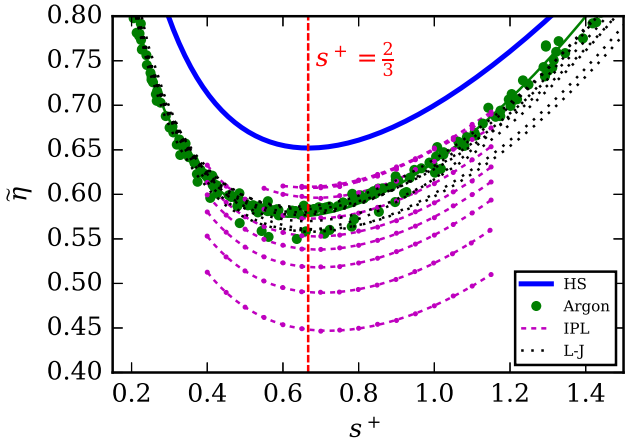

FIG. 1. Overlay of the macroscopically reduced viscosity $\widetilde{\eta}$ data for argon (see Ref. [25]), for the hard sphere from Enskog theory (HS), inverse-power-law (IPL) of hardness n_{IPL} from 6 to 52, and Lennard-Jones 12-6 (LJ) potentials at reduced temperature T^* from 1.35 to 6 studied in this work. For LJ, the curves were fit to each nominal isotherm from Ref. [26]. The IPL data are provided in the SI.

cle, T is the temperature, and ρ_{N} is the number density. The evaluation of the excess entropy for a given fluid or model potential is described below. The excess entropy can be understood as the change in the number of accessible microstates caused by interactions between the particles [22]. The interactions tend to reduce the number of accessible microstates compared with the ideal gas at the same temperature and density, and therefore the excess entropy is negative. The causal link between excess entropy and self-diffusion may be somewhat comprehensible [22] and the fluidity (reciprocal of viscosity) is proportional to self-diffusion when the Stokes-Einstein relation is applicable [23].

For simplification of the nomenclature, we define the variable $s^+ \equiv -s^{\mathrm{ex}}/k_{\mathrm{B}}$, which is a nondimensional entropy term (k_{B} is Boltzmann's constant [24]) and has the feature that it becomes more positive as the "structure" of the fluid is increased (possible microstates are reduced compared to the ideal gas at the same temperature and density).

The macroscopically scaled viscosity $\widetilde{\eta}$ is given by [13, 15]

$$\widetilde{\eta} \equiv \frac{\eta}{\rho_{\mathrm{N}}^{2/3}\sqrt{mk_{\mathrm{B}}T}} \tag{2}$$

in which η is the shear viscosity, ρ_{N} is the number density (particles per volume), m is the mass of one particle, and T is the temperature. The macroscopically scaled viscosity is a dimensionless quantity and was previously considered for a range of model potentials and selected molecular fluids [25]. In this work we extend that analysis to a more quantitative analysis of this scaling approach and place our focus on the nature of the minima of the scaled viscosity. The location of the minima of the macroscopically scaled viscosity is not coincident with the minima of the shear viscosity along an isobar [9].

Figure 1 shows selected data previously published [25] as well as a more comprehensive set of data for the inverse-power-law potentials of variable hardness generated in this work. In plotting the scaled viscosity data as a function of excess entropy, the minima of $\widetilde{\eta}$ consistently occur near the value $s^+ = 2/3$. This holds true even for rather soft inverse-power-law potentials, the Lennard-Jones fluid, and argon data covering a broad range of temperatures [25].

ATOMIC FLUID VISCOSITY

Hard sphere The hard sphere system is one of the most well-studied model potentials and forms the basis of a large body of transport property modeling as described in the review of Ref. [27], and in two of the most popular approaches for connecting the viscosity of hard spheres with those of real fluids [28–33]. From the correlations obtained from Enskog theory for the hard sphere provided by Chapman and Cowling [34, pp. 306], the viscosity values divided by the values from the fourth-order-corrected dilute-gas viscosity [34] yields (the underset annotations *kk*, *kc*, and *cc* indicate the three contributions described in the next section)

$$\frac{\eta^*}{[\eta^*_{\rho\to 0}]_4} = \underbrace{\frac{1}{g(\sigma)}}_{kk} + \underbrace{\frac{16\zeta}{5}}_{kc} + \underbrace{\frac{1}{25}\left(4 + \frac{48}{f_4\pi}\right)(4\zeta)^2 g(\sigma)}_{cc}, \tag{3}$$

where $\eta^* = \eta\sigma^2/\sqrt{m\varepsilon}$, $[\eta^*_{\rho\to 0}]_4$ is the dilute gas viscosity with fourth-order corrections, σ is the hard sphere diameter, ε is the energy scale, the packing fraction is defined by $\zeta = \pi\rho_{\mathrm{N}}\sigma^3/6$, $f_4 = 1.016$ for the fourth-order correction[34, pp. 169], and $g(\sigma)$ is the radial distribution function at contact. The hard sphere analysis is described in detail in the supporting information (Sec. 1), as well as a summary of some typographical errors in the literature, and a more concise definition of the packing fraction as a function of excess entropy. Combining the transport and thermodynamic relationships together, values of $\widetilde{\eta}$ as a function of s^+ are shown in Fig. 2. The minimum of $\widetilde{\eta}$ occurs at $s^+ = 0.668 \approx 2/3$.

Lennard-Jones 12-6 For the Lennard-Jones 12-6 fluid, there are more than two thousand data points for viscosity from molecular simulation [35], and for our purposes the most useful dataset is that of Ref. [26]. In that study, simulation data were available along nominal isotherms, and for each nominal isotherm, we calculated s^+ from the empirical equation of state [36] and applied modified entropy scaling [35] to obtain an empirical representation of $\widetilde{\eta}$; we obtained the minimum value of $\widetilde{\eta}$ along each isotherm from the empirical model. The values of $\widetilde{\eta}$ and s^+ at the minima of $\widetilde{\eta}$ are shown in Fig. 2.

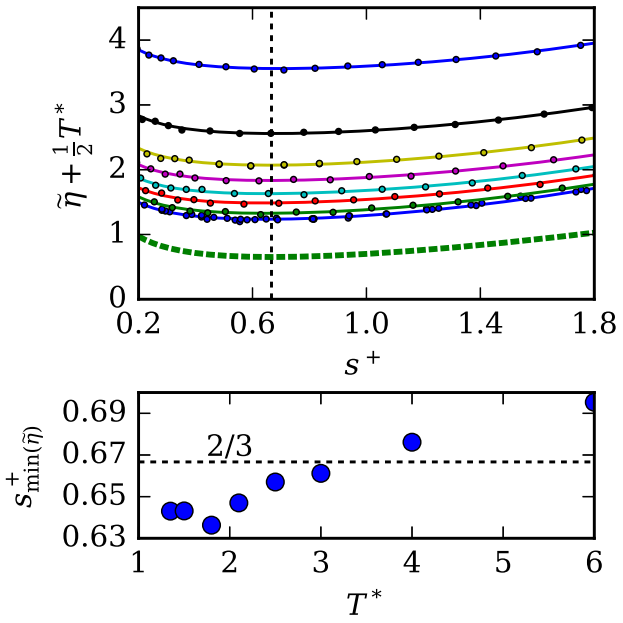

FIG. 2. Upper panel: Values of macroscopically reduced viscosity $\widetilde{\eta}$ for the hard sphere fluid from Enskog theory (thick dashed green curve) and the data for the Lennard-Jones 12-6 fluid (and the empirical curves used to locate the minima) from the equilibrium molecular dynamics simulations of [26] for the nominal isotherms of T^*=(1.35,1.5,1.8,2.1,2.5,3,4,6). The reduced temperature T^* is defined by $T^* = k_\mathrm{B}T/\varepsilon$. The values of $\widetilde{\eta}$ for the Lennard-Jones fluid are vertically shifted by $T^*/2$ so that the curves can be distinguished. Lower: Value of s^+ at the minimum of $\widetilde{\eta}$ for each nominal isotherm.

The values of s^+ at the minima of $\widetilde{\eta}$ are within the range $s^+ = 0.666 \pm 0.044 \approx 2/3$, with a slight temperature dependence.

Inverse-Power-Law For the inverse power law potential $V_\mathrm{IPL} \equiv \varepsilon(\sigma/r)^n$, where n is the hardness of the potential, molecular dynamics simulations were carried out in order to evaluate η^*. The viscosity was evaluated with the SLLOD algorithm [37] implemented in RUMD [38]. Values of s^+ are calculated from virial expansions [39] as described in the SI of Ref. 25. The IPL family includes the hard sphere in its limit of $n \to \infty$ [15], and is a common means of probing the impact of ranged repulsive interactions.

Figure 3 shows the scaled simulation results for the IPL potential calculated in this work as a function of s^+ for a range of hardnesses n. The $\widetilde{\eta}$ minima occur at values of s^+ within 10% of the hard-sphere limiting value of 2/3. In the SI (Fig. S1) the values of s^+ at the minima of $\widetilde{\eta}$ as a function of $1/n$ are shown, together with the appropriate extrapolation to the hard sphere limit.

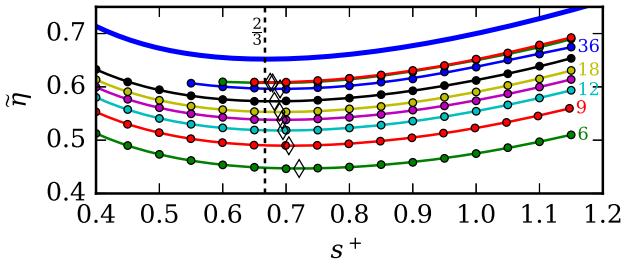

FIG. 3. Values of macroscopically reduced viscosity $\widetilde{\eta}$ for the IPL potentials of hardness n=(6,9,12,15,18,24,36,48,52) (indicated by selected labels) as a function of s^+. Diamonds indicate the interpolated minima for each hardness.

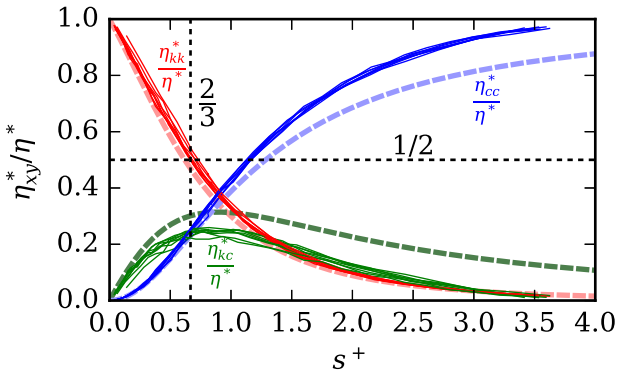

FIG. 4. Relative contributions to the scaled viscosity for the hard sphere fluid from Enskog theory (thick dashed curves) and results from Ref. [26] for the Lennard-Jones 12-6 fluid (straight line segments connecting data points along the T^*=1.35, 1.5, 1.8, 2.1, 2.5, 3, 4, and 6 nominal isotherms). The kinetic-kinetic kk term is in red, the configurational-configurational cc term is in blue, and the kinetic-configurational kc term is in green.

VISCOSITY CONTRIBUTIONS

In order to understand why the minima of $\widetilde{\eta}$ consistently occur near $s^+ = 2/3$, we start with two of the best-studied model systems: the hard sphere fluid and the Lennard-Jones 12-6 fluid. The shear viscosity can be decomposed into kinetic-kinetic (kk), kinetic-configurational (kc), and configurational-configurational (cc) contributions according to time correlation theory[26]. In some cases, the kinetic term is described as translational in the literature, and the configurational term as potential, but the definitions are identical.

For the hard sphere, the kk, kc, and cc contributions can be evaluated individually from Enskog theory (as indicated in Eq. (3)) and their relative contributions are overlaid in Fig. 4 (dashed curves) as a function of excess entropy. At zero density the kk contribution is equal to the dilute-gas contribution, and decays to zero as s^+

increases. The relative contribution from cc increases monotonically, and the coupling term has a maximum in the vicinity of $s^+ = 1$. The value of $s^+ = 2/3$ corresponds to the condition that the kk contribution represents 46.9% (nearly 50%) of the total shear viscosity.

For the Lennard-Jones 12-6 fluid, the simulations of Ref. [26] provided values for the individual contributions η^*_{kk}, η^*_{kc}, η^*_{cc} to the total shear viscosity η^* from the application of the Einstein formalism. Figure 4 shows the relative contribution to the total shear viscosity from each contribution. In the work of [26], the contributions were plotted as a function of temperature or density, resulting in a set of curves, one curve for each isotherm/isochore. The use of s^+ as the independent variable (as opposed to T or ρ_N) collapses each contribution to a single master curve. This highlights the importance of s^+ not only to the shear viscosity η^* but also for its contributions independently. Similar to the hard sphere, the value of $s^+ = 2/3$ corresponds to the relative contribution from η^*_{kk} being approximately 50% of η^*. At larger values of s^+, the quantitative behavior is somewhat different from that of the hard sphere system.

COMPARISON WITH OTHER LINES

The so-called "Widom Line" has many definitions in the literature (see for instance refs. [3, 5, 9, 12, 40–42]). The most common definition for the Widom line (here identified by WLCP) is the loci of the local maxima of the isobaric specific heat c_p originating at the critical point. One problem with this definition of a line separating the "gas" and "liquid" domains is that the Widom line terminates: the maximum disappears at temperatures that are a few times the critical temperature (e.g., see Fig. 4 of Ref. 43). Another limitation of this approach is that these maxima only occur for fluids with attraction; fully repulsive potentials have no critical point. One convenient feature of the WLCP is that it can be calculated from a thermodynamic equation of state. There have been efforts to evaluate the location of the Widom line from scattering experiments [8]. An alternative definition of the "Widom line", also applicable to fluids without attraction, is the loci of the local minima of the kinematic viscosity or thermal diffusivity along isotherms [6–8].

The "Frenkel line" [9–12] has been proposed as a variety of intrinsically inconsistent definitions of curves separating liquid-like and gas-like dynamics. These multiple definitions of the "Frenkel line" define at best a region, not a curve. Within its range of applicability, isomorph theory makes clear that at least two of the definitions of Frenkel lines are inconsistent: isomorph scaling predicts invariant dynamics along an isomorph but $c_{v,ex}$ is only constant along an isomorph to first order [44]. The theoretical underpinnings of the "Frenkel line" have been questioned in recent years [45–47].

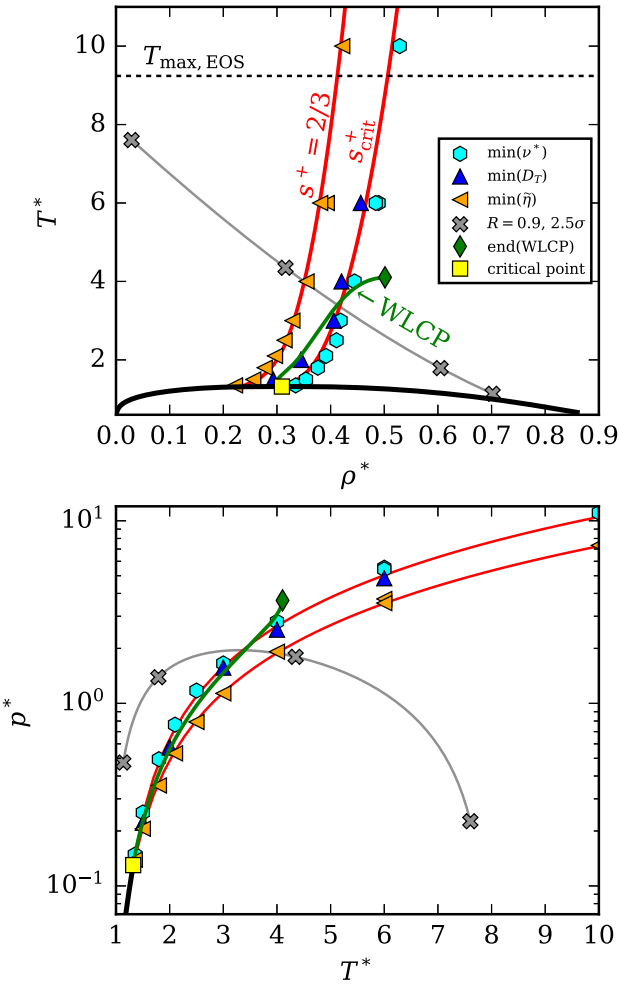

FIG. 5. The curves $s^+ = 2/3$ and s^+_{crit} and WLCP for the full L-J fluid, each evaluated from the EOS of Thol et al. [36] with $T^*_{crit} = 1.32$ and $\rho^*_{crit} = 0.31$ at the critical point in T-ρ (upper) and p-T coordinates (lower). The thick black curve is the binodal, and the grey line is a smoothed curve fit to the interpolated R=0.9 points. The minima of $\tilde{\eta}$ and ν^* are taken from interpolations of the equilibrium molecular dynamics simulations of Ref. 26 for the nominal isotherms of T^*=(1.35,1.5,1.8,2.1,2.5,3,4,6), and from non-equilibrium simulations in this work for T^*=(6,10) (tabular results in the SI, Table S3). The minima of D_T were taken from the non-equilibrium simulations of Ref. 48 for nominal isotherms of T^*=(2,3,4,6).

Figure 5 plots the curve $s^+ = 2/3$, the Widom line based upon the local maxima of the specific heat, and the curve of constant s^+ passing through the critical point. For all the calculations, the equation of state (EOS) of Ref. [36] was used, which is for the untruncated Lennard-Jones potential. This EOS is valid for temperatures up to $T^* = 9.24$, and the behavior above this limit represents extrapolation of the equation of state. The interpolated values of ρ^* at the minima of $\nu^* = \eta^*/\rho^*$ along the nominal isotherms of Meier et al. [26] were also plotted, as well as interpolated minima of the thermal diffusivity D_T

($D_T = \lambda/(\rho c_p)$, where λ is the thermal conductivity, and c_p the constant pressure specific heat) according to the simulations of Ref. 48.

The minima of $\widetilde{\eta}$ fall closely along the line $s^+ = 2/3$ (see also Fig. 2). As highlighted above (Fig. 1), the location of the minima of $\widetilde{\eta}$ occurs at roughly the same value of s^+ for potentials with and without attraction. This curve of $s^+ = 2/3$ arrives at the critical temperature at a density lower than that of the critical point. This is a philosophically unsatisfying result because the Lennard-Jones fluid has attractions between particles, and the critical point should intuitively be where the demarcation curve emanates from. On the other hand, the rule-of-thumb for application of isomorph theory is that the Pearson correlation between potential energy and virial energy should be greater than 0.9, a line also shown in the figure (interpolated from results along isochores for the Lennard-Jones potential [35], truncated at 2.5σ). The points at lower temperatures than the curve of $R = 0.9$ represent, at least approximately, state points for which isomorph theory is not expected to apply. The higher temperature points (circa $T^* > 5$) along $s^+ = 2/3$ extrapolate linearly towards the critical point. Furthermore, the location of the critical point is sensitive to the truncation of the potential; the critical temperature of the truncated and shifted Lennard-Jones fluid is approximately 80% that of the full Lennard-Jones potential [49].

The minima of thermal diffusivity and kinematic viscosity fall very closely along the line of excess entropy passing through the critical point s^+_{crit}, but are not co-incident. While the WLCP takes a different course, all the curves at least show qualitatively similar behavior – they track a curve of constant s^+. In a temperature-density representation the distinction among the "Widom lines" is clear, whereas in a temperature-pressure plot (see also Ref. 7), this distinction is more difficult to make out.

The macroscopically reduced viscosity $\widetilde{\eta}$ is an appealing quantity to consider because it is non-dimensional and is the scaled viscosity used in isomorph theory. The difference in excess entropy between the minima of ν^* and those of $\widetilde{\eta}$ is approximately constant for all temperatures, which is an interesting feature indicating a relationship between these two definitions. Isomorph theory and transport property minima appear to be intertwined at a more fundamental level than previously understood.

POLYATOMIC FLUIDS

The pair potentials described above are frequently considered models for the behavior of atomic fluids; molecular fluids have additional internal degrees of freedom. One model system that can capture (imperfectly) the impact of intramolecular degrees of freedom is the freely-jointed Lennard-Jones 12-6 chain (LJC) even if its fully-flexible bonds are not physically realistic. The transport properties of this fluid have been previously studied [48, 50, 51], and an equation of state is available for this system [52] (in combination with the appropriate monomer EOS [53]). The fully-flexible Lennard-Jones chains have been shown to have isomorphs [54, 55], so one should expect that their transport properties should also follow entropy scaling for a significant portion of their phase diagram.

Figure 6 shows the simulated values of the macroscopically-scaled transport properties along the $T^* = 3$ isotherm. A description of how the variables are defined and evaluated for LJC is given in the SI (Sec. 4.1); they are based on the mass and number density of the chains in Eq. (2). The new simulations for LJC in this work (expanding on Ref. [50]) are available in tabular form in the SI (section 4.2), as well as simulations along the $T^* = 4$ isotherm, and verification simulations at $T^* = 1$ and low density to reproduce the simulations of [56]. Molecular dynamics computations of the LJC viscosity have been performed with an in-house code already validated [51] with the Reverse Non-Equilibrium Molecular Dynamics scheme of Müller-Plathe and coworkers [57]; numerical details are provided in Hoang et al. [58]. In order to obtain the location of the minima, a polynomial was fit to $\ln(\widetilde{\eta} \times (s^+)^{2/3})$ for each chain (application of modified entropy scaling proposed in Ref. [35]), and the empirical function was then used to locate the minimum of $\widetilde{\eta}$.

Figure 7 shows the values of the excess entropy at the minima of $\widetilde{\eta}$ for each chain length M. While there is some noise caused by the interpolation scheme (and the simulations themselves), the excess entropy values at the minima of $\widetilde{\eta}$ are very nearly a linear function of the chain length M. Unfortunately, simulation data passing through the minima are only available for the $T^* = 3$ and $T^* = 4$ isotherms (simulation data at higher densities for a wider range of temperatures are available in Ref. 51). In other words, the LJC model fluid shows that there is a linear relationship between the molecular size of the fluid and the excess entropy at which the change between gas-like and liquid-like behavior occurs. This notion aligns with the link between excess entropy and lacunarity (roughly speaking, lacunarity is a quantification of the amount of void space within a continuous medium) [59, 60].

In this figure the values of s^+ calculated at the critical points were also overlaid in order to demonstrate corresponding states between the minima of $\widetilde{\eta}$ and the values of s^+ calculated at the critical points. We calculated vapor-liquid equilibria from the equation of state (see the SI, Fig. S2) from which we calculated critical points consistent with the thermodynamic model. Other critical points are given in the literature (e.g., [58, 61]), but they do not provide values of s^+. Aside from the monomer/polymer jump (M going from 1 to 2), the s^+

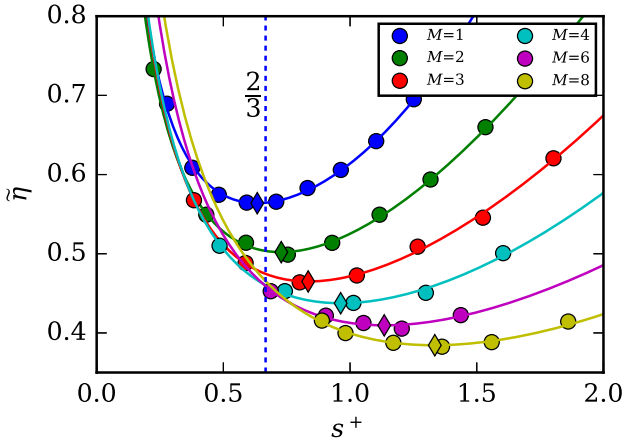

FIG. 6. The values of $\widetilde{\eta}$ along the $T^* = 3$ isotherm for the freely-jointed Lennard-Jones chains with M segments. The solid curves indicate the modified entropy scaling curves used to obtain the minima, the diamonds indicate the interpolated minima.

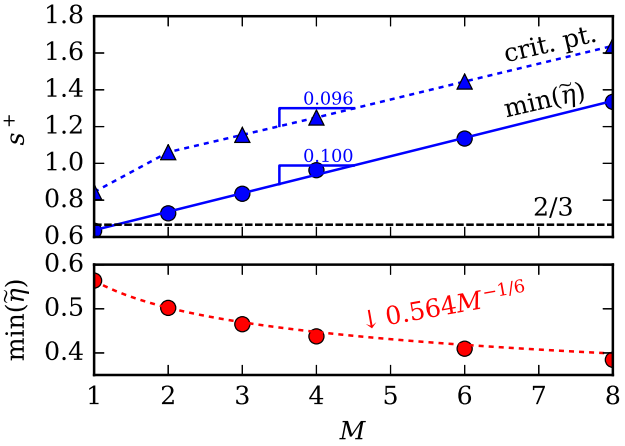

FIG. 7. Upper panel: Values of s^+ at the minima of $\widetilde{\eta}$ for the freely-jointed Lennard-Jones chains with M segments along T^*=3 (filled circles) and at the respective critical point for the LJ chains (filled triangles). The slopes of each curve are indicated by the number above the slope symbol. Lower panel: Values of the the minima of $\widetilde{\eta}$ for the LJ chains with M segments along T^*=3.

values at the minima of $\widetilde{\eta}$ shift systematically with the values of s^+ calculated at the critical points.

For LJC, the values of the minima along isotherms follow the empirical scaling $\min(\widetilde{\eta}) \propto M^{-1/6}$, where the proportionality constant is the value of $\min(\widetilde{\eta})$ for the monomer. This exponent of $1/6$ on M is unlike the Rouse [62] or Zimm [63] models; the difference is related to the use of macroscopic scaling, which introduces a factor of M in the number density term of $\widetilde{\eta}$. The dilute-gas viscosity scales with $M^{-1/2}$ [50], and that of the liquid, according to Rouse scaling, scales with M, therefore, it follows that the behavior at the minima is intermediate between these two limits.

CONCLUSIONS

In this work we showed that excess entropy has an even more intimate connection with the macroscopically-scaled transport properties than previously described. The line $s^+ = 2/3$ for atomic fluids can be straightforwardly calculated from a thermodynamic equation of state, and corresponds to the case that the kinetic-kinetic contribution to viscosity is approximately equal to one half of the total viscosity. For all fluids, lines of constant s^+ can be unambiguously evaluated from an equation of state or from molecular dynamics simulations and can be used as a demarcating curve between gas-like and liquid-like behaviors. Indeed, it can be used to define a demarcation line between gas-like and liquid-like fluid behaviors for fluids possessing, or not, attractive interactions. Furthermore, we show that the minima of kinematic viscosity and thermal diffusivity track closely the curve of constant excess entropy passing through the critical point, providing further evidence for the importance of the excess entropy to the dynamics.

Considering the modified entropy scaling in Ref. [35] for the Lennard-Jones fluid, it seems highly likely that a similar analogy can be made to thermal conductivity and self-diffusion. Viscosity is simpler than the other transport properties in some regards, as it does not have the complication of a meaningful critical enhancement (as in the case of thermal conductivity), and the scaled dilute gas values are much smaller in magnitude than those of the liquid phase (unlike self-diffusion). A consideration of these other transport properties in the same framework is merited.

This work has benefited enormously from generous brainstorming and discussion with many people. We would especially like to thank: our past and present colleagues at NIST (Eric Lemmon, Chris Muzny, Allan Harvey, Richard Messerly, and Arno Laesecke), Jeppe Dyre, John O'Connell, Ulrich Deiters, Jadran Vrabec, Michal Roth, and Vincent Arp. Special thanks are also due to an anonymous reviewer who led us to revisit the minima of thermal diffusivity and kinematic viscosity. This work was supported by a research grant (00023189) from VILLUM FONDEN.

SUPPLEMENTARY MATERIAL

The supplementary material includes mathematical derivations that complement the analysis in this manuscript, tabular simulation results, and additional figures for completeness.

* ian.bell@nist.gov; Corresponding author
† guillaume.galliero@univ-pau.fr
‡ stephanie.delage@univ-pau.fr
§ lorenzoc@ruc.dk

[1] T. Andrews, XVIII. The Bakerian Lecture – On the continuity of the gaseous and liquid states of matter, Philos. Trans. Roy. Soc. London **159**, 575 (1869).
[2] P. Schienbein and D. Marx, Investigation concerning the uniqueness of separatrix lines separating liquidlike from gaslike regimes deep in the supercritical phase of water with a focus on Widom line concepts, Phys. Rev. E **98**, 10.1103/physreve.98.022104 (2018).
[3] V. V. Brazhkin, Y. D. Fomin, A. G. Lyapin, V. N. Ryzhov, and E. N. Tsiok, Widom Line for the Liquid–Gas Transition in Lennard-Jones System, J. Phys. Chem. B **115**, 14112 (2011).
[4] P. F. McMillan and H. E. Stanley, Going supercritical, Nature Physics **6**, 479 (2010).
[5] H.-O. May and P. Mausbach, Riemannian geometry study of vapor-liquid phase equilibria and supercritical behavior of the Lennard-Jones fluid, Phys. Rev. E **85**, 031201 (2012).
[6] T. Bryk, F. Gorelli, G. Ruocco, M. Santoro, and T. Scopigno, Collective excitations in soft-sphere fluids, Phys. Rev. E **90**, 10.1103/physreve.90.042301 (2014).
[7] F. A. Gorelli, T. Bryk, M. Krisch, G. Ruocco, M. Santoro, and T. Scopigno, Dynamics and thermodynamics beyond the critical point, Scientific Reports **3**, 10.1038/srep01203 (2013).
[8] G. G. Simeoni, T. Bryk, F. A. Gorelli, M. Krisch, G. Ruocco, M. Santoro, and T. Scopigno, The Widom line as the crossover between liquid-like and gas-like behaviour in supercritical fluids, Nat. Phys. **6**, 503 (2010).
[9] V. V. Brazhkin, A. G. Lyapin, V. N. Ryzhov, K. Trachenko, Y. D. Fomin, and E. N. Tsiok, Where is the supercritical fluid on the phase diagram?, Phys. Usp. **55**, 1061 (2012).
[10] V. V. Brazhkin, Y. D. Fomin, A. G. Lyapin, V. N. Ryzhov, and K. Trachenko, Two liquid states of matter: A dynamic line on a phase diagram, Phys. Rev. E **85**, 10.1103/physreve.85.031203 (2012).
[11] V. V. Brazhkin, Y. D. Fomin, A. G. Lyapin, V. N. Ryzhov, E. N. Tsiok, and K. Trachenko, "Liquid-Gas" Transition in the Supercritical Region: Fundamental Changes in the Particle Dynamics, Phys. Rev. Lett. **111**, 10.1103/physrevlett.111.145901 (2013).
[12] Y. D. Fomin, V. N. Ryzhov, E. N. Tsiok, and V. V. Brazhkin, Thermodynamic properties of supercritical carbon dioxide: Widom and Frenkel lines, Phys. Rev. E **91**, 10.1103/physreve.91.022111 (2015).
[13] Y. Rosenfeld, Relation between the transport coefficients and the internal entropy of simple systems, Phys. Rev. A **15**, 2545 (1977).
[14] J. C. Dyre, Perspective: Excess-entropy scaling, J. Chem. Phys. **149**, 210901 (2018).
[15] J. C. Dyre, Simple liquids' quasiuniversality and the hard-sphere paradigm, J. Phys.: Condens. Matter **28**, 323001 (2016).
[16] N. P. Bailey, U. R. Pedersen, N. Gnan, T. B. Schrøder, and J. C. Dyre, Pressure-energy correlations in liquids. I. Results from computer simulations, J. Chem. Phys. **129**, 184507 (2008).
[17] N. P. Bailey, U. R. Pedersen, N. Gnan, T. B. Schrøder, and J. C. Dyre, Pressure-energy correlations in liquids. II. Analysis and consequences, J. Chem. Phys. **129**, 184508 (2008).
[18] N. Gnan, T. B. Schrøder, U. R. Pedersen, N. P. Bailey, and J. C. Dyre, Pressure-energy correlations in liquids. IV. "Isomorphs" in liquid phase diagrams, J. Chem. Phys. **131**, 234504 (2009).
[19] T. B. Schrøder, N. P. Bailey, U. R. Pedersen, N. Gnan, and J. C. Dyre, Pressure-energy correlations in liquids. III. Statistical mechanics and thermodynamics of liquids with hidden scale invariance, J. Chem. Phys. **131**, 234503 (2009).
[20] T. B. Schrøder, N. Gnan, U. R. Pedersen, N. P. Bailey, and J. C. Dyre, Pressure-energy correlations in liquids. V. Isomorphs in generalized Lennard-Jones systems, J. Chem. Phys. **134**, 164505 (2011).
[21] D. M. Heyes, D. Dini, L. Costigliola, and J. C. Dyre, Transport coefficients of the Lennard-Jones fluid close to the freezing line, J. Chem. Phys. **151**, 204502 (2019).
[22] J. R. Errington, T. M. Truskett, and J. Mittal, Excess-entropy-based anomalies for a waterlike fluid, J. Chem. Phys. **125**, 244502 (2006).
[23] L. Costigliola, D. M. Heyes, T. B. Schrøder, and J. C. Dyre, Revisiting the Stokes-Einstein relation without a hydrodynamic diameter, J. Chem. Phys. **150**, 021101 (2019).
[24] P. J. Mohr, D. B. Newell, B. N. Taylor, and E. Tiesinga, Data and analysis for the CODATA 2017 special fundamental constants adjustment, Metrologia **55**, 125 (2018).
[25] I. H. Bell, Probing the link between residual entropy and viscosity of molecular fluids and model potentials, Proc. Natl. Acad. Sci. U.S.A. **116**, 4070 (2019).
[26] K. Meier, A. Laesecke, and S. Kabelac, Transport coefficients of the Lennard-Jones model fluid. I. Viscosity, J. Chem. Phys. **121**, 3671 (2004).
[27] C. M. Silva and H. Liu, Theory and Simulation of Hard-Sphere Fluids and Related Systems (Springer-Verlag, 2008) Chap. Modelling of Transport Properties of Hard Sphere Fluids and Related Systems, and its Application, pp. 383–492.
[28] M. Assael, J. Dymond, M. Papadaki, and P. Patterson, Correlation and prediction of dense fluid transport coefficients, Fluid Phase Equilib. **75**, 245 (1992).
[29] M. J. Assael, J. H. Dymond, M. Papadaki, and P. M. Patterson, Correlation and prediction of dense fluid transport coefficients. III. n-alkane mixtures, Int. J. Thermophys. **13**, 659 (1992).
[30] M. J. Assael, J. H. Dymond, and P. M. Patterson, Correlation and prediction of dense fluid transport coefficients. IV. A note on diffusion, Int. J. Thermophys. **13**, 729 (1992).
[31] M. J. Assael, J. H. Dymond, and P. M. Patterson, Correlation and prediction of dense fluid transport coefficients. V. Aromatic hydrocarbons, Int. J. Thermophys. **13**, 895 (1992).
[32] V. Vesovic and W. A. Wakeham, The prediction of the viscosity of dense gas mixtures, Int. J. Thermophys. **10**, 125 (1989).
[33] V. Vesovic and W. Wakeham, Prediction of the viscosity of fluid mixtures over wide ranges of temperature and pressure, Chem. Eng. Sci. **44**, 2181 (1989).

[34] S. Chapman and T. G. Cowling, *The Mathematical Theory of Non-uniform Gases: An Account of the Kinetic Theory of Viscosity, Thermal Conduction and Diffusion in Gases* (Cambridge University Press, 1970).

[35] I. H. Bell, R. Messerly, M. Thol, L. Costigliola, and J. Dyre, Modified Entropy Scaling of the Transport Properties of the Lennard-Jones Fluid, J. Phys. Chem. B , 6345 (2019).

[36] M. Thol, G. Rutkai, A. Köster, R. Lustig, R. Span, and J. Vrabec, Equation of State for the Lennard-Jones Fluid, J. Phys. Chem. Ref. Data **45**, 023101 (2016).

[37] D. J. Evans and G. P. Morriss, *Statistical Mechanics of Nonequilibrium Liquids* (Academic Press, 1990) p. 302.

[38] Available at http://www.rumd.org.

[39] N. S. Barlow, A. J. Schultz, S. J. Weinstein, and D. A. Kofke, An asymptotically consistent approximant method with application to soft- and hard-sphere fluids, J. Chem. Phys. **137**, 204102 (2012).

[40] N. J. Hestand and J. L. Skinner, Perspective: Crossing the Widom line in no man's land: Experiments, simulations, and the location of the liquid-liquid critical point in supercooled water, J. Chem. Phys. **149**, 140901 (2018).

[41] A. R. Imre, C. Ramboz, U. K. Deiters, and T. Kraska, Anomalous fluid properties of carbon dioxide in the supercritical region: application to geological CO_2 storage and related hazards, Environ. Earth Sci. **73**, 4373 (2014).

[42] A. Imre, U. Deiters, T. Kraska, and I. Tiselj, The pseudocritical regions for supercritical water, Nucl. Eng. Des. **252**, 179 (2012).

[43] S. Pieprzyk, A. C. Brańka, S. Maćkowiak, and D. M. Heyes, Comprehensive representation of the Lennard-Jones equation of state based on molecular dynamics simulation data, J. Chem. Phys. **148**, 114505 (2018).

[44] T. B. Schrøder and J. C. Dyre, Simplicity of condensed matter at its core: Generic definition of a Roskilde-simple system, J. Chem. Phys. **141**, 204502 (2014).

[45] T. Bryk, F. A. Gorelli, I. Mryglod, G. Ruocco, M. Santoro, and T. Scopigno, Behavior of Supercritical Fluids across the 'Frenkel Line', J. Phys. Chem. Lett. **8**, 4995 (2017).

[46] V. V. Brazhkin, C. Prescher, Y. D. Fomin, E. N. Tsiok, A. G. Lyapin, V. N. Ryzhov, V. B. Prakapenka, J. Stefanski, K. Trachenko, and A. Sapelkin, Comment on "Behavior of Supercritical Fluids across the 'Frenkel Line'", J. Phys. Chem. B **122**, 6124 (2018).

[47] T. Bryk, F. A. Gorelli, I. Mryglod, G. Ruocco, M. Santoro, and T. Scopigno, Reply to "Comment on 'Behavior of Supercritical Fluids across the Frenkel Line'", J. Phys. Chem. B **122**, 6120 (2018).

[48] G. Galliero and C. Boned, Thermal conductivity of the Lennard-Jones chain fluid model, Phys. Rev. E **80**, 061202 (2009).

[49] M. Thol, G. Rutkai, R. Span, J. Vrabec, and R. Lustig, Equation of State for the Lennard-Jones Truncated and Shifted Model Fluid, Int. J. Thermophys. **36**, 25 (2015).

[50] S. Delage Santacreu, G. Galliero, M. Odunlami, and C. Boned, Low density shear viscosity of Lennard-Jones chains of variable rigidities, J. Chem. Phys. **137**, 204306 (2012).

[51] G. Galliero and C. Boned, Shear viscosity of the Lennard-Jones chain fluid in its gaseous, supercritical, and liquid states, Phys. Rev. E **79**, 021201 (2009).

[52] J. K. Johnson, E. A. Mueller, and K. E. Gubbins, Equation of State for Lennard-Jones Chains, J. Phys. Chem. **98**, 6413 (1994).

[53] J. Kolafa and I. Nezbeda, The Lennard-Jones fluid: an accurate analytic and theoretically-based equation of state, Fluid Phase Equilib. **100**, 1 (1994).

[54] A. A. Veldhorst, J. C. Dyre, and T. B. Schrøder, Scaling of the dynamics of flexible Lennard-Jones chains, J. Chem. Phys. **141**, 054904 (2014).

[55] A. A. Veldhorst, J. C. Dyre, and T. B. Schrøder, Scaling of the dynamics of flexible Lennard-Jones chains: Effects of harmonic bonds, J. Chem. Phys. **143**, 194503 (2015).

[56] P. V. Ramírez-González and V. A. Escobar-Barrios, Viscosity and normal stress forces of Lennard-Jones chains using reverse non-equilibrium molecular dynamics, Mol. Phys. **115**, 2970 (2017).

[57] F. Müller-Plathe, Reversing the perturbation in nonequilibrium molecular dynamics: An easy way to calculate the shear viscosity of fluids, Phys. Rev. E **59**, 4894 (1999).

[58] H. Hoang, S. Delage-Santacreu, and G. Galliero, Simultaneous Description of Equilibrium, Interfacial, and Transport Properties of Fluids Using a Mie Chain Coarse-Grained Force Field, Ind. Eng. Chem. Res. **56**, 9213 (2017).

[59] E. Detmar, S. Y. Nezhad, and U. K. Deiters, Determination of the Residual Entropy of Simple Mixtures by Monte Carlo Simulation, Langmuir **33**, 11603 (2017).

[60] S. Y. Nezhad and U. K. Deiters, Estimation of the entropy of fluids with Monte Carlo computer simulation, Mol. Phys. **115**, 1074 (2016).

[61] F. A. Escobedo and J. J. D. Pablo, Simulation and prediction of vapour-liquid equilibria for chain molecules, Mol. Phys. **87**, 347 (1996).

[62] P. E. Rouse, A Theory of the Linear Viscoelastic Properties of Dilute Solutions of Coiling Polymers, J. Chem. Phys. **21**, 1272 (1953).

[63] B. H. Zimm, Dynamics of Polymer Molecules in Dilute Solution: Viscoelasticity, Flow Birefringence and Dielectric Loss, J. Chem. Phys. **24**, 269 (1956).